DOI:
10.1002/jbm.a.35017

Document Version
Peer reviewed version

Citation for published version (APA):
Martinez, J. O., Evangelopoulos, M., Chiappini, C., Liu, X., Ferrari, M., & Tasciotti, E. (2013). Degradation and biocompatibility of multistage nanovectors in physiological systems: Degradation and Biocompatibility of MSV. *Journal of Biomedical Materials Research - Part A*, *102*(10), 3540-3549. https://doi.org/10.1002/jbm.a.35017

Published in final edited form as:
J Biomed Mater Res A. 2014 October ; 102(10): 3540–3549. doi:10.1002/jbm.a.35017.

Degradation and biocompatibility of multi-stage nanovectors in physiological systems

Jonathan O. Martinez[1,2], **Michael Evangelopoulos**[1], **Ciro Chiappini**[1,3,#], **Xuewu Liu**[1], **Mauro Ferrari**[1], and **Ennio Tasciotti**[1,†]

[1]Department of Nanomedicine, The Methodist Hospital Research Institute, 6670 Bertner Ave., Houston, TX 77030, USA

[2]Graduate School of Biomedical Sciences, University of Texas Health Science Center, 6767 Bertner Ave., Houston, TX 77030, USA

[3]Department of Biomedical Engineering, University of Texas at Austin, 107 W. Dean Keeton, Austin, TX 78712, USA

Abstract

The careful scrutiny of drug delivery systems is essential to evaluate and justify their potential for the clinic. Among the various studies necessary for pre-clinical testing, the impact of degradation is commonly overlooked. In this paper, we investigate the effect of fabrication (porosity and nucleation layer) and environment (buffer and pH) factors on the degradation kinetics of multi-stage nanovectors (MSV) composed of porous silicon. The degradation by-products of MSV were exposed to endothelial cells and analyzed for detrimental effects on cellular internalization, architecture, proliferation, and cell cycle. Increases in porosity resulted in accelerated degradation exhibiting smaller sized particles at comparable times. Removal of the nucleation layer (thin layer of small pores formed during the initial steps of etching) triggered a premature collapse of the entire central porous region of MSV. Variations in buffers prompted a faster degradation rate yielding smaller MSV within faster time frames while increases in pH stimulated erosion of MSV and thus faster degradation. In addition, exposure to these degradation by-products provoked negligible impact on the proliferation and cell cycle phases on primary endothelial cells. Here, we propose methods that lay the foundation for future investigations towards understanding the impact of the degradation of drug delivery platforms.

Keywords

Degradation; Porous Silicon; Multistage Nanovectors; Drug Delivery; Cytocompatibility

[†]To whom correspondence should be addressed: Dr. Ennio Tasciotti, Department of Nanomedicine, The Methodist Hospital Research Institute, 6670 Bertner Ave. MS R7-414 Houston, TX 77030 (USA), etasciotti@tmhs.org, Tel: + 1 713 441 7319.
[#]Current Address: Department of Materials, Imperial College London, Prince Consort Rd, London, SW7 2AZ, UK

1. Introduction

In the past decade, porous silicon (pSi) has gained significant momentum within the biomedical field due to desirable traits such as favorable degradability[1], biocompatibility[2], and photoluminescence.[3] These unique set of qualities allowed pSi to be applied to applications ranging from optics[4] and biosensors[5] to microelectronics[6] and tissue engineering.[7,8] Moreover, the flexible nature of pSi permits the adjustment of fabrication parameters to modify precise characteristics (e.g., size, shape, surface, pore size) and has made pSi particularly favorable for drug delivery applications. For example, by leveraging the increased surface area and pore volume of pSi vectors, the secure attachment and incorporation of various molecules, therapeutic moieties, and nanoparticles was successfully achieved.[9–11] This inherent versatility allowed pSi vectors to increase the bioavailability, drug solubility, and provide prolonged release of various payloads.[12]

pSi has the unique ability to degrade completely yielding a bioinert[13] silicic acid as its only product. As demonstrated in previous studies, silicic acid is fundamental for normal bone homeostasis and increased levels of silicic acid were well sustained within the body and readily excreted through urine.[14] In addition, advantageous health benefits have been witnessed in silicic acid's rare ability to reduce aluminum uptake and promote increased excretion of aluminum in urine[15] which can be beneficial for the prevention and progression of Alzheimer's disease.[16] Previous studies have also demonstrated silicic acid's ability to stimulate the synthesis of collagen type 1 and promote osteoblastic differentiation.[17] These many advantages provided by pSi by-products allow pSi to be a suitable material for drug delivery applications.

Thus by taking advantage of the numerous features of pSi, our group successfully engineered[18] and tested[19–21] multi-stage nanovectors (MSV) whose primary objective was to decouple the multiplicity of tasks required for the delivery of therapeutics to specific locations and distribute them onto separate stages. Within this platform, pSi performs as the first stage and is tasked to carry, protect, deliver, and release the second stage in an efficient manner. The adjustment of fabrication parameters enables the creation of pore sizes ranging from 3–100 nm in diameter to accommodate the loading of various sized payloads.[18] Additionally, to ensure increased retention within the pores, a nucleation layer is incorporated to prevent payloads from passing freely through the pores. Although both properties serve to enable the greatest efficacy of a payload-loaded MSV, the characteristics that regulate their degradation have yet to be fully investigated.

In addition to efficiency and safety, a major consideration for drug delivery systems is their ability to be compatible within the body's environmental conditions and maintain stability for systemic administration. While previous work examined the degradation effect of pegylation[22] and biofluids[23] on pSi, this work aims to investigate the degradation dynamics of MSV to understand their stability at different porosities, removal of the nucleation layer, and impact of buffer and pH. Furthermore, the consequences of MSV degradation by-products on cellular architecture, proliferation, and cell cycle were explored. Herein, we monitored the impact of fabrication (porosity, nucleation layer) and environmental (buffer, pH) parameters on the degradation of MSV using Inductively Coupled Plasma - Atomic

Emission Spectrometer (ICP-AES), scanning electron microscopy (SEM), flow cytometry, and size and zeta potential analysis. In addition, the cyto-compatibility of MSV was assessed using primary cells to assess detrimental effects on cell structure, proliferation, and cell cycle.

2. Materials & Methods

2.1 MSV Fabrication

We previously reported how combining microfabrication with electrochemical etching yielded the MSV[18] used in this study (Figure 1). An initial deposition of a 120 nm thick layer of silicon-rich silicon nitride (SiN) over a 100 mm p-type Si wafer (Figure 1A) followed by photolithography yielded an array of 2 μm diameter holes with 2 μm pitch (Figure 1B). Reactive ion etching (RIE) in CF_4 gas formed 400 nm deep trenches in the Si corresponding to the photolithographic holes (Figure 1C). Stripping of photoresist followed by electrochemical etching with the SiN masking layer formed MSV in the 2 μm×400 nm trenches (Figure 1D). The current profile during electrochemical etching and the composition of the etch solution determined the porosity and shell thickness of the MSV. A two-step current process yielded MSV with small to large pores (SP-LP, respectively, Figure 1C). The initial step used a lower current to form the nucleation layer and following host layer. The nucleation layer was a < 50 nm thick layer of pores < 2 nm in diameter that inevitably forms in the initial steps of electrochemical etch. A step up in current formed an unstable pSi layer with high porosity between the host layer and the solid silicon substrate. Once the electrochemical process was completed, the substrates were washed and dried in N_2. At this step it was possible to remove the nucleation layer, if desired, through a short RIE in CF_4 gas (Figure 1E). Release of MSV from the substrate was achieved by shattering the release layer through sonication in isopropanol (Figure 1F). XLP MSV consisting exclusively of a host layer were not mechanically stable, due to the >80% porosity of the layer. For this reason the formation of MSV with XL pores instead required the initial formation of a transitional layer with ~80nm thickness having pores of progressively increasing diameter, which varied from that of the nucleation layer to that of the XLP host layer (Figure 1C). To achieve this, an initial step with progressively increasing current was introduced before the two-step current process. These studies were conducted using 3.2 × 0.7 μm MSV with various porosities dependent on study.

2.2 Degradation of MSV

MSV with varying porosities and presence of a nucleation layer was studied by inducing degradation in PBS under rotation using a LabQuake tube rotator at 10 rpm and 37 °C, pH 7.2.[24] At pre-determined times, aliquots were removed from samples, centrifuged at 4200 rpm for 10 minutes, and supernatants were discarded. Aliquots were stored at 4 °C until analysis could be performed. NP, SP, MP, LP, and XLP were used to study the effect of porosity and MP were selected to study the contribution of a nucleation layer. Effect due to buffers was investigated comparing Tris-HCl 20 mM pH 7.3 + 0.9% NaCl (Sigma-Aldrich) as the ‘saline’ solution and Dulbecco’s modified eagle medium (GIBCO) supplemented with 10% fetal bovine serum (GIBCO) as the ‘cell culture media’ (CCM) solution. To investigate the effect of buffer, SP and LP MSV were selected to have a range of MSV porosities tested.

1.2×10^7 MSV (SP & LP) were suspended in 1.5 mL of saline or CCM solution, and measured in triplicate. Degradation was studied as previously mentioned with samples under rotation at 10 rpm at 37°C. One rotational speed was chosen to concentrate on the differences between fabrication and environmental factors rather than the effect rotation may have. The effect attributed to pH was investigated by adjusting 20 mM Tris-HCl to various pH levels. 1.5×10^6 LP MSV were suspended in 1.5 mL of each pH and rotated at 37°C.

For flow cytometry, aliquots were re-suspended in deionized water and measured using a BD FACSCalibur (BD Biosciences) and analyzed with CellQuest. For ICP-AES, aliquots were placed in nylon centrifugal filter tubes (0.45 μm, VWR) and centrifuged for 10 minutes at 4200 rpm. Samples were diluted 1:100 in water containing 1 ppm of Yttrium and measured on a Varian Vista Pro Simultaneous Axial at the Geochemistry Laboratory at Rice University. MSV size distribution and number were examined using the Z2™ COULTER COUNTER® Cell and Particle Counter outfitted with a 50 μm ampoule aperture tube (Beckman Coulter; Fullerton, CA). Samples were diluted into 1.0 mL of ISOTON and counted using limits of 1.0 to 2.8 μm, with the resulting data exported to Excel. Samples for SEM were washed twice in water to remove salts from samples and re-suspended in 25 μL of water and placed in the center of an aluminum stage. Samples were left to dry overnight in a vacuum desiccator. Images were taken on a Zeiss Neon 40 microscope equipped with an in-lens detector. Zeta potential measurements were resuspended in 1.5 mL of filtered monobasic PB (10 mM, pH 7.4) and measured using a ZetaPALS analyzer (Brookhaven Instruments Corporation; Holtsville, NY).

2.3 Cell culture

Human Umbical Vein Endothelial Cells (HUVEC) were purchased from Lonza (Lonza Group Ltd; Switzerland) and cultured in Clonetics ® EBM®-2 Endothelial Cell Growth Medium-2 (Lonza; CC-3156) supplemented with EGM-2 SingleQuots® Kit (Lonza; CC-4176). HUVEC were used between passages 4–10 for described experiments.

2.4 MTT & Cell cycle

For MTT, HUVEC were seeded in 96 well plates at 5,000 cells per plate. Degradation byproducts collected from the supernatant of completely degraded MSV were added to each well. At pre-determined times, wells were incubated with 3-[4,5-Dimethylthiazol-2-yl]-2,5-Diphenyltetrazolium Bromide (MTT) at 0.5 mg/mL in complete media for two hours at 37 °C, 5% CO_2 followed by an 30 minute incubation with DMSO and measured for absorbance at 570 nm on a BioTek plate reader.

The effect on cell cycle after treatment with the by-products of degradation from MSV was evaluated as previously described.[25] Briefly, HUVEC were treated with SP or LP MSV degraded by-products by completely degrading MSV and removing samples from the degraded supernatant portion (i.e., not partially degraded MSV). At pre-determined times, cells were collected and quickly fixed using 70% ethanol at 4°C for 10 minutes then stored at −20°C for 30 minutes. A 50 μg/mL solution of propidium iodide (PI) was prepared in a 10 mM Tris buffer at pH 7.3 containing 5mM $MgCl_2$. One mL of PI solution and 50 μL of a 1.5 mg/mL solution of RNAse I were slowly added under gentle agitation. Cells were incubated

for 1 hour at 37 °C, followed by three washes PBS, re-suspended in 200 μL and analyzed using a Becton Dickinson FACSCalibur.

2.5 HUVEC cytoskeletal staining

HUVEC were seeded into a chamber slide (LabTek) at 75,000 cells per well and allowed to adhere overnight. The following day, HUVEC were treated with DyLightÆ 555 MSV at a ratio of 1:10 and an equivalent amount of MSV fragments (i.e., partially degraded MSV) for 24 hours. HUVEC were then stained with AlexaFluor 488 Phalloidin (Invitrogen), mounted with Pro Long Gold containing DAPI, and imaged using an inverted Nikon Eclipse Ti microscope.

2.6 Statistical Analysis

All statistics were calculated using Prism GraphPad software. Zeta Potential values were tested using a Two-Way ANOVA followed by a Bonferroni post-test to compare NP to SP and MP. Nonlinear regression analysis fitted with a one phase association equation using the least squares method was used to test significance in ICP-AES data (Figure 3D and Figure 4A). Constraints of Y_0 at 0.0 and Plateau equal to 100 were used and the resulting rate constants were compared using an extra sum of squares F test. For MTT results (Figure 6), linear regression analysis was performed and significance was determined by testing whether the slopes and intercepts were significantly different (F test). In all cases: * was used for p-values between 0.01 to 0.05, ** for values between 0.001 to 0.01, and *** for values < 0.001.

3.0 Results & Discussion

3.1 Impact of porosity on MSV degradation

The flexible nature of MSV allows for tunable porosity to accommodate a variety of payloads and thus can have critical implications for drug delivery. This impact was studied by comparing five different conditions (Table 1): NP (non-porous), SP (small pores), MP (medium pores), LP (large pores), and XLP (extra large pores). Differences in degradation profiles were investigated using size and zeta potential analysis at several times. Figure 2A compared the volume distributions of various MSV at different time points. The distributions were offset on the y-axis for clarity and to compare the changes in size at different times. The initial peak at 1 fL was the detection limit of the instrument and was common to all MSV examined. As MSV degraded, a shift in their volume towards the detection peak is apparent for all MSV with the exception of NP. These shifts appeared earlier for MSV with higher porosities and whose peaks progressed closer to the detection limit at a faster rate. Figure 2B substantiates this claim by normalizing to zero hours and plotting the modes (e.g., highest occurring number) collected during volume analysis. As time increased, we observed the same trend as the volume graphs where the more porous MSV displayed an overall smaller size at each time point while NP experienced minimal changes in size. For example, at 24 hours the size of MSV had decreased by 37%, 56%, 62%, and 70%, respectively, for SP, MP, LP, and XLP.

Zeta potential measurements were performed to determine the surface charge of MSV as they degraded. Figure 2C diagramed the changes in surface charge of NP, SP, and MP MSV during degradation. Due to their APTES modification, MSV were initially imparted with a positive charge (+10–15 mV) and with time MSV became highly negative (−25–30 mV). At eight hours, MSV reached a plateau of negative charge of −40mV and −35mV for NP and SP/MP, respectively. By 24 hours, the surface charges of SP and MP were neutral while NP remained negative (significantly different from SP and MP). Hence as the porosity of MSV increased, an equivalent increase in degradation rate was observed. Surface charge measurements revealed that the APTES surface modification quickly degraded and exhibited a pattern such that the highest value was achieved at eight hours potentially indicating the point where the highest surface area existed. On the other hand, the surface charge measurements of NP MSV remained consistent confirming minimal degradation over time.

3.2 Absence of nucleation layer and effect on pore structure

A critical function for MSV is to load and retain a nanoparticle payload within its porous structure. The nucleation layer serves to prevent payloads from passing freely through MSV and is typically associated with pore sizes less than 2 nm. We investigated the impact on MSV degradation by comparing SEM, ICP-AES, flow cytometry, and size analysis. SEM images illustrated that MSV without a nucleation layer (MSVxNL) began with larger pores on the front-side while retaining the same overall shape compared to regular MSV (Fig 3A). The overall shape of MSV and MSVxNL remained similar over time. However, we observed that the porous structure of MSVxNL displayed significant remodeling such that by 18 hours considerably larger pores were observed. This resulted in premature pore instability ultimately triggering their complete collapse by 24 hours (Fig 3A). As shown in Figure 3B, the size distribution of MSVxNL began with slightly smaller sizes consistent with the earlier results of higher porosity MSV. The shifts in size over time associated with MSVxNL were comparable to the variations observed in conventional MSV containing a nucleation layer. Flow cytometry (Fig 3C) confirmed that MSVxNL size (forward scatter, FSC) and shape (side scatter, SSC) degraded in a manner consistent with classical MSV. FSC and SSC contour and 3D plots illustrated similar patterns with analogous shifts accumulating at the origin of the graphs, indicative of MSV degradation between 24 and 48 hours. In addition, ICP-AES (Fig 3D) confirmed that MSVxNL had minimal effect on the overall degradation of MSV as no significant increase in Si was detected in solution determined using nonlinear regression analysis and comparing rate constants. The absence of a nucleation layer from MSV had a negligible effect on their overall degradation pattern resulting in comparable changes in size and shape. However, the porous structure of MSV experienced a remarkable difference in their degradation displaying increased instability generating increased porosity in the core of MSV resulting in complete pore collapse by 24 hours. Although the absence of a nucleation layer may negatively impact payload loading or retention, it may be beneficial in order to achieve a quicker release rate attributed to the quicker pore break-down observed.

3.3 Degradation behavior of MSV in varying buffers

An understanding of the interplay between the local environment and the effect on the degradation of drug delivery vectors is vital to gauge its use for systemic administration. To this extent, we compared the degradation kinetics of MSV in two different types of buffers: DMEM with 10% FBS (CCM) and Tris-HCl + 0.9% NaCl (Saline), both at pH 7.3. SP and LP MSV were investigated to discover the impact of buffer on degradation using ICP-AES, SEM, and size analysis. Figure 4A demonstrated that when suspended in CCM, the overall degradation process was accelerated for both SP and LP. In CCM, SP reached a plateau of maximum Si deposition by 24 hours, while in saline this was not achieved till 48 hours (90% at 24 hours). Similarly, LP reached plateaus at 18 hours in CCM and 48 hours in saline (80% at 24 hours). Nonlinear regression analysis revealed that MSV in CCM experienced a significant acceleration in degradation rate, such that they degraded more than 3.5× faster in CCM compared to saline for both SP and LP. Furthermore, SEM images (Fig 4B) confirmed that both SP and LP degraded quicker in CCM compared to saline. In CCM, MSV exhibited dramatic transformations in the overall appearance displaying smaller sized particles at 18 and 24 hours for SP and 12 versus 24 hours for LP. Figure 4C validated that dramatic shifts in size were observed for MSV in different buffers. Both SP and LP in CCM experienced a substantial shift within five hours resulting in acquisition of MSV predominantly at the lower detection limit, which was not the case for MSV in saline. Thus, MSV exposed to CCM revealed accelerated degradation kinetics resulting in substantial structural instability and shifts in size compared to MSV in saline buffers. The addition of amino acids and serum proteins commonly found in CCM[26] and FBS possibly contributed to increased degradation. The disparity between CCM and saline suggests that MSV will experience a significant increase in degradation upon encountering sites rich in proteins, amino acids, and salts such as the tissue and cellular microenvironment and during systemic blood circulation.

3.4 pH-induced degradation of MSV

Comprehension of the degradation phenomenon governing MSV in varying pH environments is essential to ensure stability during systemic administration and upon interactions within cellular environments. The influence of pH on MSV degradation was investigated using a range from 9–12. In alkaline solutions, the adsorption of hydroxyl ions on Si produces its dissolution into orthosilicic acid as the concentration of hydroxyl ions are increased.[27] This favors the formation of a bioinert neutral monomer of silicate ions as equilibrium is reached that plays a beneficial role in the optimal growth of bone and collagen.[28] MSV degradation in alkaline conditions can be represented as shown in Figure 5A. In an aqueous solution, the hydroxyl layer of the MSV undergoes weak nucleophilic attack by the water molecules. Increasing the pH of the solution, therefore, provides a stronger nucleophilic attack that ultimately produces accelerated degradation of MSV into silicic acid. As shown in Figure 5B, the contour plots acquired by flow cytometry displayed progressive loss of organization of the overall shape and size of MSV as pH increased, indicated by the increase of particles located outside the gating box. The ROI box within the plots was used to monitor the extent of degradation, such that as MSV degrade their distribution will extend outside of the box and drift towards the origin where small fragments accumulate. MSV experienced substantial effects on the size and shape in 24 h dependent on the pH used. At pH 12, MSV began drifting at 2.5 hours while at pH 10

manifestations were not apparent until 20 hours. Next, we compared the total counts collected by the flow cytometer at various times (Figure 5C). This was performed by fitting the data using a plateau followed by a one-phase exponential decay constraining the plateau to 0 and Y_0 to 100, complete parameters detailed in supplementary information. At increasing pH, MSV revealed an accelerated degradation with fewer MSV collected at increasing pH levels. We fitted the data using a plateau followed by a one-phase exponential decay constraining the plateau to 0 and Y_0 to 100. This resulted in distinct degradation rate constants of 0.053, 0.306, 0.638, 4.45 h^{-1} for pH 9, 10, 11, 12, respectively. In addition, this model calculated delays in the initiation of degradation (X0) such that as the pH increased the decay began earlier with times ranging from 1.2 to 8.6 hours. Taken together, this data demonstrated that the increasing concentrations of hydroxide ions resulted in a rapid degradation on the surface of MSV producing considerable structural modifications. As the solution became more basic, the strength of the nucleophilic attack intensified resulting in an overall increase in exposed pSi surface area and ultimately yielding the final product of orthosilicic acid.

3.5 Cellular uptake and architecture

The concerns regarding the exposure of nanovectors to healthy cells must be adequately examined in order to gauge its potential use in the clinic. We investigated the reaction of HUVEC cultures upon introduction to partially degraded MSV (i.e. fragments). We initially sought to understand the impact the internalization of fragments have on the cell architecture, specifically inspecting the microfilaments of the cytoskeleton. Hence, we compared the f-actin staining of HUVEC treated with equal concentrations of intact MSV and MSV fragments. As shown in Figure 6A, the microtubules (green) and nucleus (blue) of HUVEC displayed similar staining, comparing untreated and MSV. HUVEC exhibited conserved parallel filamentous microfilament arrangements that assembled equally throughout the entire cell. Previous studies demonstrated that MSV were quickly delivered to the perinuclear region.[25] Similarly, MSV fragments were found to preferentially accumulate around the perinuclear area. Furthermore, nuclear staining revealed consistent shapes upon internalization indicating a negligible cytotoxic effect attributed to fragments. Thus, internalization of MSV degradation by-products exhibited a negligible effect on cellular architecture producing conventional endothelial phenotypes.

3.6 Maintained cellular integrity

Understanding the potential consequences of complete degradation by-products on normal cellular homeostasis is crucial for evaluating drug delivery vectors. The impact of degradation products on the proliferation and cell cycle maintenance of HUVEC was investigated by exposing cells to completely degraded MSV. The proliferation of HUVEC was studied by comparing the incorporation of MTT to extrapolate the level of metabolic activity. Degraded products from oxidized and APTES MSV exhibited similar proliferation rates when compared to PBS controls (Fig. 6B). HUVEC displayed a resilient response to the degradation by-products of MSV of varying porosities (SP, MP, LP, XLP) preserving an active mitochondrial function. In addition, linear regression analysis revealed that the proliferation rates (i.e., slopes) of HUVEC exposed to oxidized and APTES modified MSV were not significantly different than the PBS control. The different porosities demonstrated

that HUVEC tolerated a wide concentration of Si approximately ranging from 30 to 80 pg/cell for XLP to SP, respectively.

Although comprehending the metabolic activity and continued proliferation of cells is useful, it fails to provide detailed information on specific events occurring within cells upon exposure. As shown in Figure 6C, we quantified the percentage of HUVEC within the different phases of the cell cycle at 48 hours comparing the effect of degradation products with different surface chemistry and porosities. HUVEC revealed equivalent patterns of distribution across the phases at 48 hours with similar quantities among the different groups. A comparison of these results with control and intact MSV[25] revealed that at 48 hours HUVEC exposed to the degradation products of MSV behaved nearly identical. Control HUVEC displayed 17% in the sub G_0 phase, commonly where apoptotic/inactive cells are categorized, comparable with cells containing MSV degradation products whose values ranged from 15–21%. Furthermore an inspection of combined effort of the G_2/M and S phases of the cycle, representative of mitotic and DNA replication, respectively, can be used to chronicle the 'active' fraction of cell division. Using this benchmark, we confirmed that HUVEC preserved these routine functions in a consistent manner displaying 32% for control cells and ranging from 28–34% for MSV degradation. In addition, analogous HUVEC percentages were discovered in the G_0/G_1 phase, which recognizes cells in the resting/checkpoint stage. Hence, exposure to MSV degradation products yielded a negligible cellular response from primary endothelial cells. In fact, we recently demonstrated that intact MSV would permit HUVEC and stem cells to conserve their intrinsic functions (e.g., tube formation and multipotent differentiation) upon internalization confirming a higher degree of biocompatibility.[29] Here, HUVEC maintained proliferation and routine cycling through various cellular phases without influencing DNA replication for several days after the introduction of the degradation products.

4. CONCLUSION

In summary, we have reported how MSV were influenced by both fabrication and environmental elements and how the degradation products affected normal cellular viability and integrity. This study can potentially serve as a model on how to characterize drug delivery vectors in order to achieve optimal degradation profiles while maintaining minimal impact on biological systems. Variations in MSV porosity resulted in substantial shifts in size and shape producing faster degrading MSV as the porosity increased. The removal of the nucleation layer greatly impacted the stability of pore structure generating an early collapse of the pores. Environmental influences also dictated how MSV would behave such that buffers containing amino acids and proteins (e.g., cell culture media) and an increase in pH facilitated quicker degradation of MSV. The degradation by-products of MSV were well tolerated and exhibited minimal effect on the cellular architecture, proliferation, and cell cycle progression of HUVEC. The work presented here establishes a precedent for future studies to investigate the impact the degradation of drug delivery vectors has on biological systems.

Supplementary Material

Refer to Web version on PubMed Central for supplementary material.

Acknowledgments

The authors would like to thank Glen Snyder (Rice University) for sample measurement by ICP-AES, David Haviland (TMHRI) for flow cytometry assistance, Matthew Landry (TMHRI) for excellent graphical support, and Kevin Plant for technical assistance. This research was supported by The Alliance for NanoHealth, specifically DOD TATRC grants W81XWH-09-2-0139 and W81XWH- 10-2-0125; and internal support provided by TMHRI including the Ernest Cockrell Jr. Distinguished Endowed Chair. In addition, JOM was supported by a 5F31CA154119-02 NIH pre-doctoral fellowship.

REFERENCES

1. Canham LT. Bioactive silicon structure fabrication through nanoetching techniques. Advanced Materials. 1995; 7(12):1033–1037.
2. Bayliss SC, Heald R, Fletcher DI, Buckberry LD. The Culture of Mammalian Cells on Nanostructured Silicon. Advanced Materials. 1999; 11(4):318–321.
3. Pavesi L, Ceschini M, Rossi F. Photoluminescence of porous silicon. Journal of Luminescence. 1993; 57(1–6):131–135.
4. Pavlikov AV, Lartsev AV, Gayduchenko IA, Yu Timoshenko V. Optical properties of materials based on oxidized porous silicon and their applications for UV protection. Microelectronic Engineering. 2012; 90(0):96–98.
5. Ko PJ, Ishikawa R, Takamura T, Morimoto Y, Cho B, Sohn H, Sandhu A. Porous-Silicon Photonic-Crystal Platform for the Rapid Detection of Nano-Sized Superparamagnetic Beads for Biosensing Applications. Nanoscience and Nanotechnology Letters. 2011; 3(5):612–616.
6. Bogaerts W, De Heyn P, Van Vaerenbergh T, De Vos K, Kumar Selvaraja S, Claes T, Dumon P, Bienstman P, Van Thourhout D, Baets R. Silicon microring resonators. Laser & Photonics Reviews. 2012; 6(1):47–73.
7. Sun W, Puzas JE, Sheu T-J, Fauchet PM. Porous silicon as a cell interface for bone tissue engineering. physica status solidi (a). 2007; 204(5):1429–1433.
8. Coffer JL, Whitehead MA, Nagesha DK, Mukherjee P, Akkaraju G, Totolici M, Saffie RS, Canham LT. Porous silicon-based scaffolds for tissue engineering and other biomedical applications. physica status solidi (a). 2005; 202(8):1451–1455.
9. Wu EC, Park J-H, Park J, Segal E, Cunin Fdr, Sailor MJ. Oxidation-Triggered Release of Fluorescent Molecules or Drugs from Mesoporous Si Microparticles. ACS Nano. 2008; 2(11): 2401–2409. [PubMed: 19206408]
10. Salonen J, Laitinen L, Kaukonen AM, Tuura J, Björkqvist M, Heikkilä T, Vähä-Heikkilä K, Hirvonen J, Lehto VP. Mesoporous silicon microparticles for oral drug delivery: Loading and release of five model drugs. Journal of Controlled Release. 2005; 108(2–3):362–374. [PubMed: 16169628]
11. Parodi A, Quattrocchi N, van de Ven AL, Chiappini C, Evangelopoulos M, Martinez JO, Brown BS, Khaled SZ, Yazdi IK, Enzo MV, Isenhart L, Ferrari M, Tasciotti E. Synthetic nanoparticles functionalized with biomimetic leukocyte membranes possess cell-like functions. Nat Nanotechnol. 2013; 8(1):61–68. [PubMed: 23241654]
12. Prestidge CA, Barnes TJ, Lau CH, Barnett C, Loni A, Canham L. Mesoporous silicon: a platform for the delivery of therapeutics. Expert Opin Drug Deliv. 2007; 4(2):101–110. [PubMed: 17335408]
13. Low SP, Voelcker NH, Canham LT, Williams KA. The biocompatibility of porous silicon in tissues of the eye. Biomaterials. 2009; 30(15):2873–2880. [PubMed: 19251317]
14. Jurkic LM, Cepanec I, Pavelic SK, Pavelic K. Biological and therapeutic effects of ortho-silicic acid and some ortho-silicic acid-releasing compounds: New perspectives for therapy. Nutr Metab (Lond). 2013; 10(1):2. [PubMed: 23298332]

15. Jugdaohsingh R, Reffitt DM, Oldham C, Day JP, Fifield LK, Thompson RP, Powell JJ. Oligomeric but not monomeric silica prevents aluminum absorption in humans. Am J Clin Nutr. 2000; 71(4): 944–949. [PubMed: 10731501]

16. Kawahara M, Kato-Negishi M. Link between Aluminum and the Pathogenesis of Alzheimer's Disease: The Integration of the Aluminum and Amyloid Cascade Hypotheses. Int J Alzheimers Dis. 2011; 2011:276393. [PubMed: 21423554]

17. Reffitt DM, Ogston N, Jugdaohsingh R, Cheung HF, Evans BA, Thompson RP, Powell JJ, Hampson GN. Orthosilicic acid stimulates collagen type 1 synthesis and osteoblastic differentiation in human osteoblast-like cells in vitro. Bone. 2003; 32(2):127–135. [PubMed: 12633784]

18. Chiappini C, Tasciotti E, Fakhoury JR, Fine D, Pullan L, Wang YC, Fu L, Liu X, Ferrari M. Tailored porous silicon microparticles: fabrication and properties. Chemphyschem. 2010; 11(5): 1029–1035. [PubMed: 20162656]

19. Tasciotti E, Liu X, Bhavane R, Plant K, Leonard AD, Price BK, Cheng MM-C, Decuzzi P, Tour JM, Robertson F, Ferrari M. Mesoporous silicon particles as a multistage delivery system for imaging and therapeutic applications. Nat Nano. 2008; 3(3):151–157.

20. Ananta JS, Godin B, Sethi R, Moriggi L, Liu X, Serda RE, Krishnamurthy R, Muthupillai R, Bolskar RD, Helm L, Ferrari M, Wilson LJ, Decuzzi P. Geometrical confinement of gadolinium-based contrast agents in nanoporous particles enhances T1 contrast. Nat Nanotechnol. 2010; 5(11): 815–821. [PubMed: 20972435]

21. Tanaka T, Mangala LS, Vivas-Mejia PE, Nieves-Alicea R, Mann AP, Mora E, Han HD, Shahzad MM, Liu X, Bhavane R, Gu J, Fakhoury JR, Chiappini C, Lu C, Matsuo K, Godin B, Stone RL, Nick AM, Lopez-Berestein G, Sood AK, Ferrari M. Sustained small interfering RNA delivery by mesoporous silicon particles. Cancer Res. 2010; 70(9):3687–3696. [PubMed: 20430760]

22. Godin B, Gu J, Serda RE, Bhavane R, Tasciotti E, Chiappini C, Liu X, Tanaka T, Decuzzi P, Ferrari M. Tailoring the degradation kinetics of mesoporous silicon structures through PEGylation. J Biomed Mater Res A. 2010; 94(4):1236–1243. [PubMed: 20694990]

23. Bimbo LM, Makila E, Laaksonen T, Lehto VP, Salonen J, Hirvonen J, Santos HA. Drug permeation across intestinal epithelial cells using porous silicon nanoparticles. Biomaterials. 2011; 32(10):2625–2633. [PubMed: 21194747]

24. Martinez JO, Chiappini C, Ziemys A, Faust AM, Kojic M, Liu X, Ferrari M, Tasciotti E. Engineering multi-stage nanovectors for controlled degradation and tunable release kinetics. Biomaterials. 2013; 34(33):8469–8477. [PubMed: 23911070]

25. Martinez JO, Boada C, Yazdi IK, Evangelopoulos M, Brown BS, Liu X, Ferrari M, Tasciotti E. Short and Long Term, In Vitro and In Vivo Correlations of Cellular and Tissue Responses to Mesoporous Silicon Nanovectors. Small. 2012

26. Genzel Y, Konig S, Reichl U. Amino acid analysis in mammalian cell culture media containing serum and high glucose concentrations by anion exchange chromatography and integrated pulsed amperometric detection. Anal Biochem. 2004; 335(1):119–125. [PubMed: 15519579]

27. Sailor, MJ. Fundamentals of Porous Silicon Preparation. Porous Silicon in Practice. Wiley-VCH: Verlag GmbH & Co. KGaA; 2011. p. 1-42.

28. Carlisle EM. Silicon: an essential element for the chick. Science. 1972; 178(4061):619–621. [PubMed: 5086395]

29. Martinez JO, Parodi A, Liu X, Kolonin MG, Ferrari M, Tasciotti E. Evaluation of Cell Function Upon Nanovector Internalization. Small. 2012

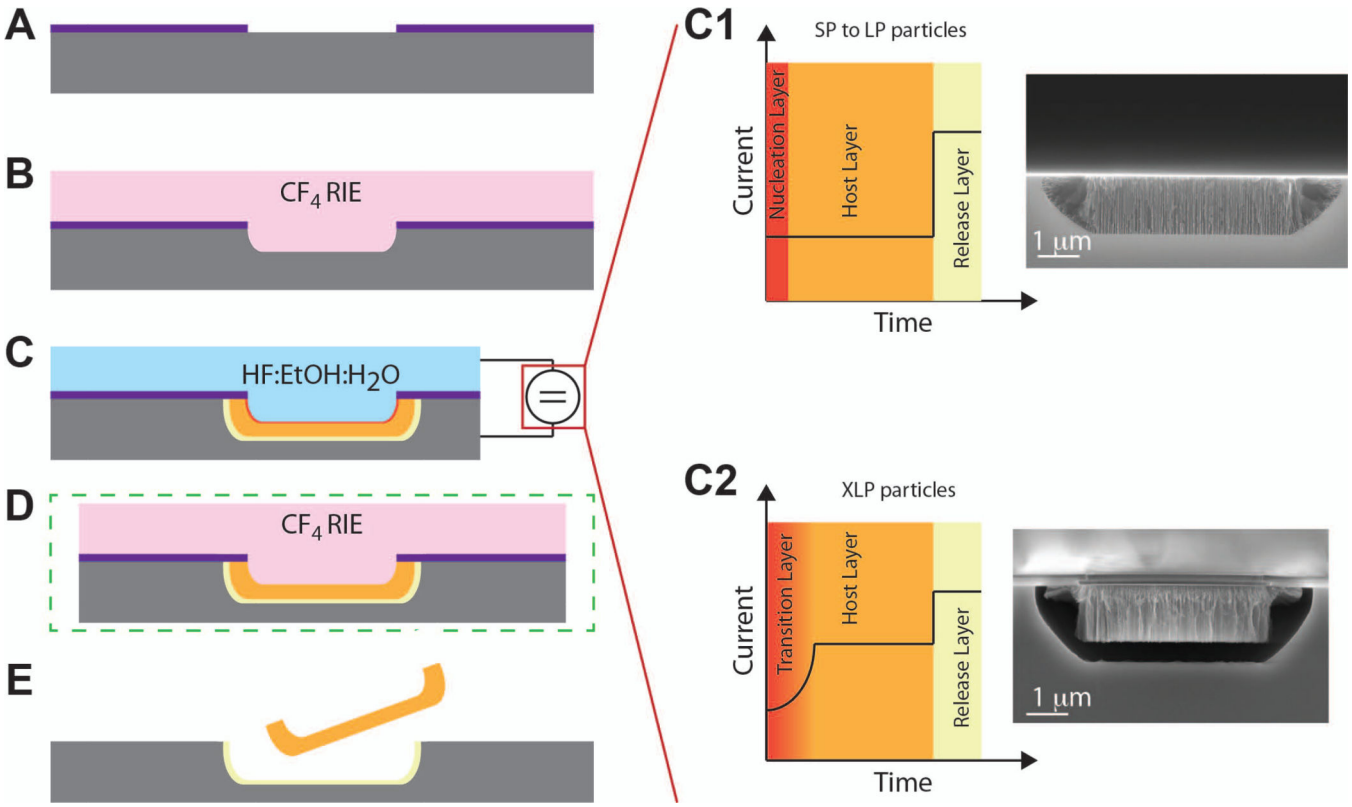

Figure 1. Schematic representation of the MSV fabrication process

A) Fabrication began with a silicon rich silicon nitride layer. B) Patterning in CF4 yielded an array of 2 μm diameter holes with pitch of 2 μm. C) A reactive ion etch formed pores corresponding to photolithographic holes from the previous step. Graphs on right show the effect of current applied over time for SP to LP (top) and XLP (bottom) with SEM images depicting porosity. D) The optional removal of the nucleation layer was performed in a reactive ion etch with CF_4. E) MSV particles were released after etch with CF_4.

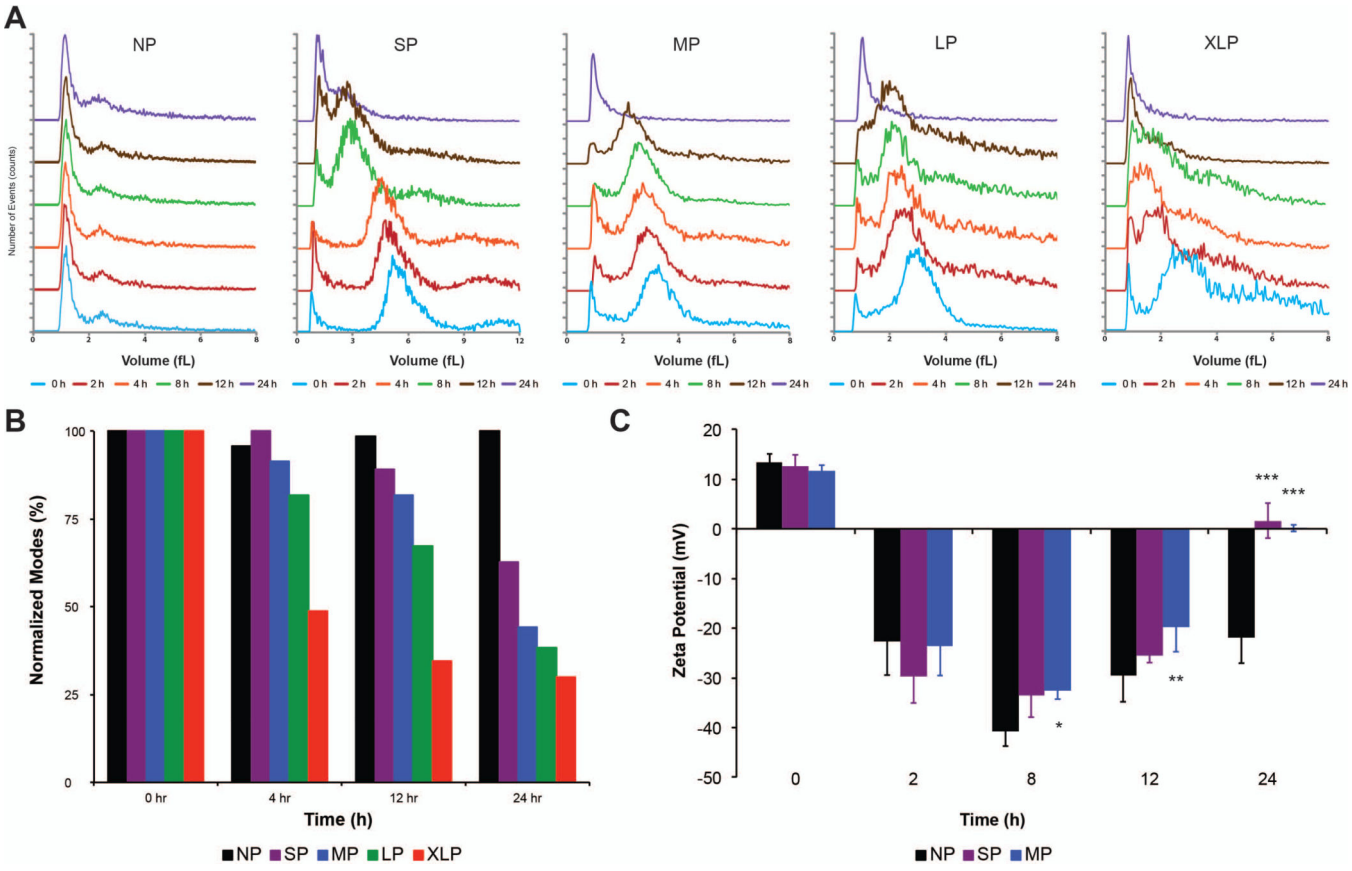

Figure 2. Effect of porosity on degradation of MSV

A) Volume distributions of MSV with varying porosities are plotted at various times comparing the shifts in size. Distributions are offset on the y-axis to highlight differences between time points. B) The mode, or the value that appears most frequent, at each time point is plotted and compared to other porosities of MSV. NP serves as control, as degradation of non-porous silicon particles is minimal and was used for comparison. C) Zeta potential measurements were used to provide insight on the surface charge of NP, SP, and MP MSV. The results are shown as mean ± SD. Asterisks denote data points where the difference was statistically significant compared to NP. * $p < 0.05$, ** $p < 0.01$, *** $p < 0.001$.

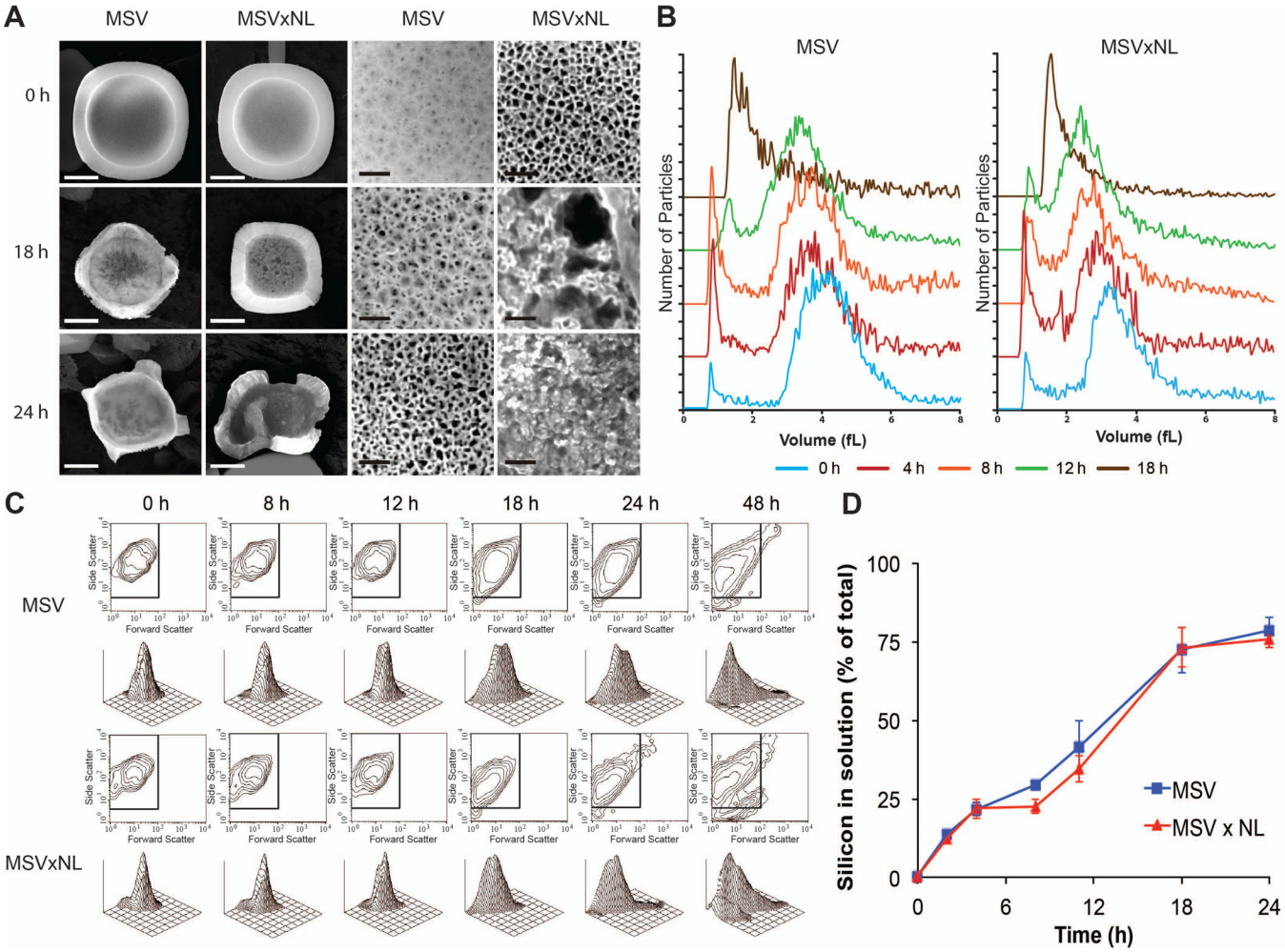

Figure 3. The impact of the nucleation layer on pore stability

A) MSV with and without a nucleation layer (MSVxNL) were compared at various times looking at the overall effect on size and shape (left) and their pores (right) on the front-side where the nucleation layer is visible. Scale bars, left for particle is 1 *m; right for pores is 50 nm. B) Volume distribution of MSV and MSVxNL showing smaller sized for MSVxNL but with comparable shifts in size with increased time. C) Flow cytometry verifying similar patterns for size (forward scatter) and shape (side scatter) of the two MSV. D) ICP-AES contrasting MSV versus MSVxNL to confirm minimal change in overall degradation of MSV without nucleation layer.

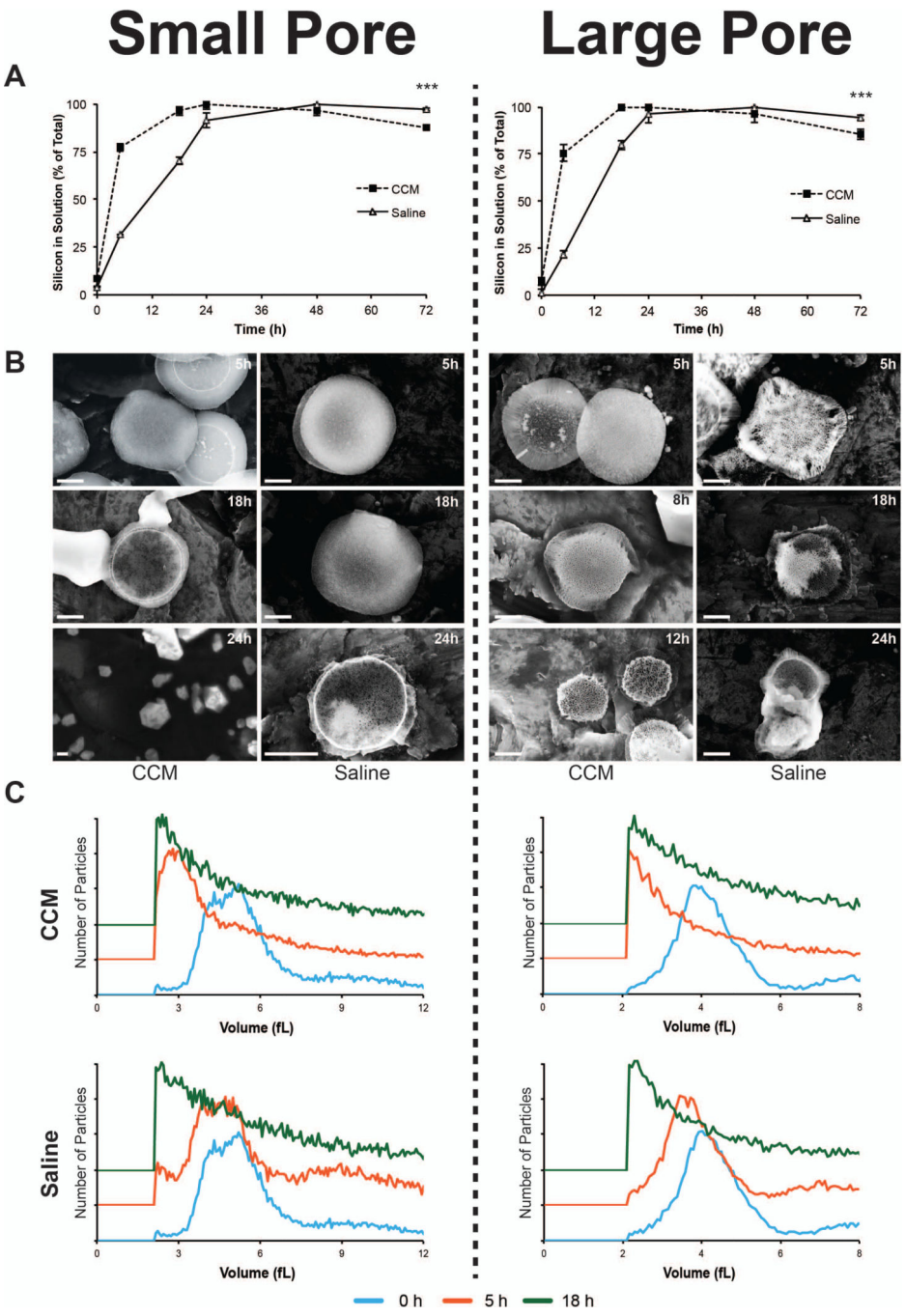

Figure 4. Influence of buffer in degradation of MSV

A) ICP-AES comparison of MSV, SP (left column) and LP (right column), degradation in CCM and saline solution. B) SEM images showing MSV degradation in CCM (left) and saline (right) solutions at various time points. C) Volume distributions of MSV in CCM (top) and saline (bottom) are plotted at various time points relating the shifts in size. Distributions are offset on the yaxis to highlight differences between time points. The results are shown as mean ± SD. Asterisks denote where the difference was statistically significant compared to Saline. *** $p < 0.001$.

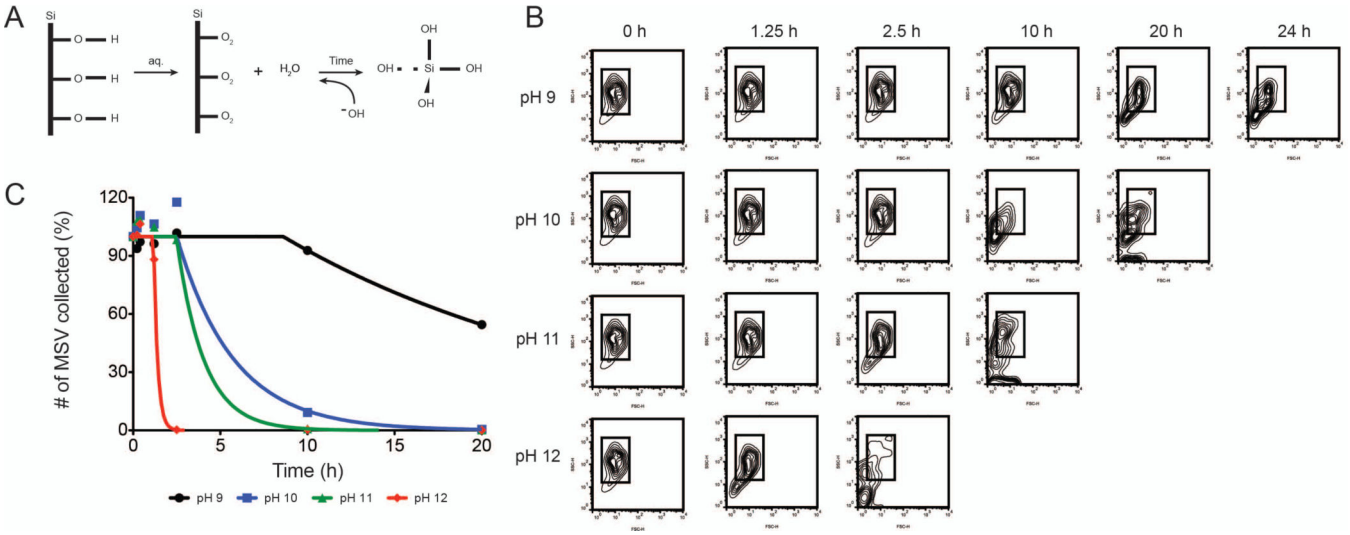

Figure 5. Degradation effect of MSV in varying pH environments

A) Schematic showing possible interactions between the MSV surface and hydroxyl groups. Hydroxyl ions of an alkaline solution weaken the surface of the MSV forming bioinert silicic acid. B) Flow cytometry exhibiting distinct patterns and changes in size (forward scatter) and shape (side scatter) exposed to the varying pH environments. C) Flow cytometer counts collected at various time points to show degradation rates of MSV at pHs between 9 and 12.

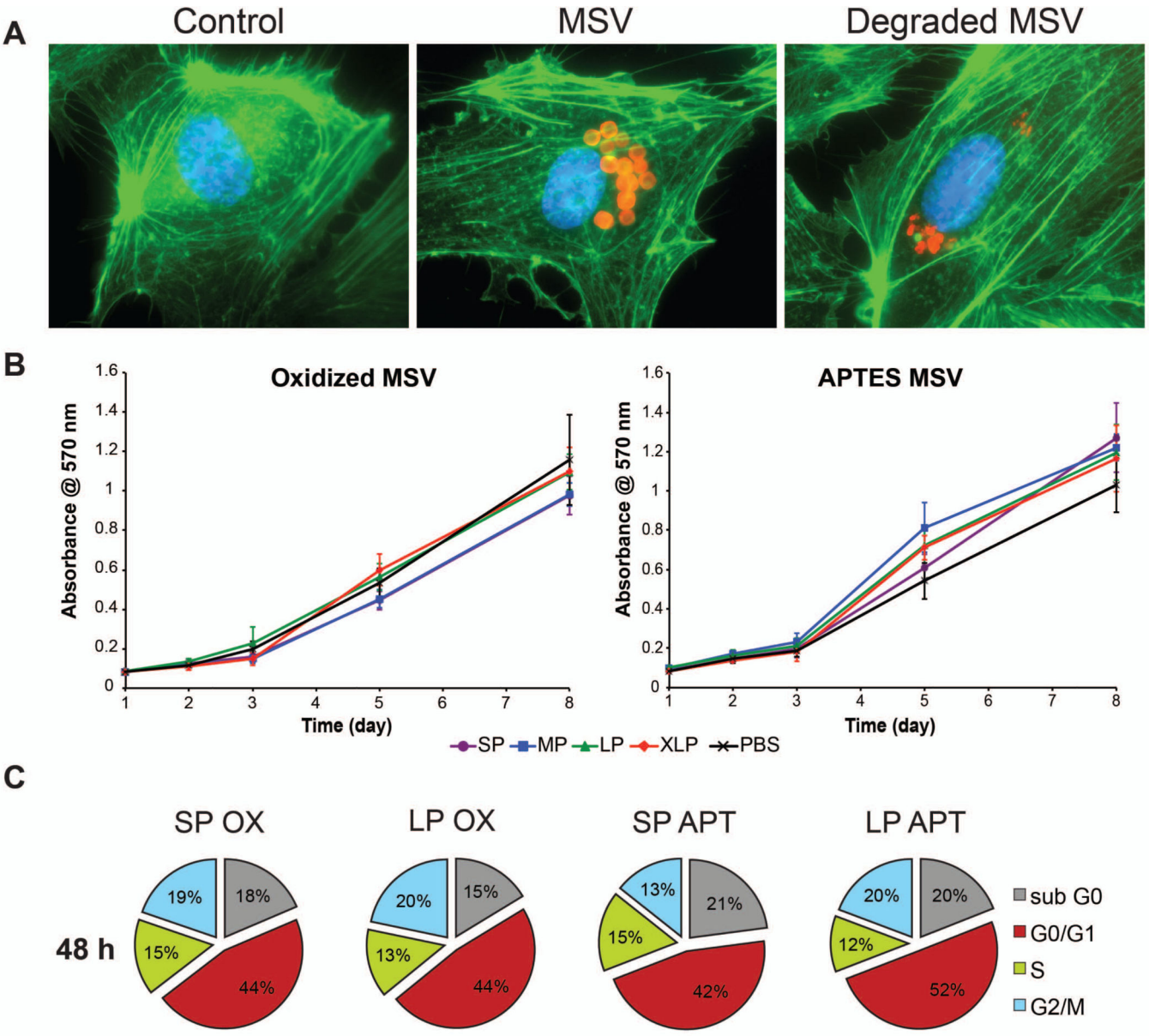

Figure 6. Cellular architecture and biocompatibility of MSV degradation products

A) The microfilaments (green) and nucleus (blue) of HUVEC were stained to interpret the effect of exposing MSV fragments. Control and non-degraded MSV were used to compare cytoskeletal structure. B) An MTT assay to demonstrate the continued proliferation of HUVEC after internalizing oxidized (left) and APTES (right) degradation products of MSV with varying porosities (SP-XLP). Proliferation of HUVEC was compared to sterile PBS, the buffer used to degrade the MSV. The results are shown as mean ± SD. C) Cell cycle analysis at 48 hours after introduction to degradation products of MSV. The cell cycle of HUVEC was conserved independent of surface (oxidized and APTES) and porosity (SP and LP).

Table 1

MSV Characteristics

Name of MSV	Porosity (%)	Pore size (nm)
Non-Porous (NP)	0	0
Small Pore (SP)	46	10.1
Medium Pore (MP)	51	15.2
Large Pore (LP)	66	26.3
Extra Large Pore (XLP)	82	51.3